

Viscoelastic Parameter Identification based Structure-Thermal Analysis of Rubber Bushing

Haiyan H Zhang¹

¹ Purdue University, US

Received: 16 December 2013 Accepted: 1 January 2014 Published: 15 January 2014

Abstract

Rubber bushing, working as flexible connection parts or vibration isolators, is widely used in commercial vehicles, airplane, and off-highway transportation. The appropriate mathematical modeling of it in proper vehicle simulation is becoming more and more demanding recently. This paper focuses on viscoelastic parameter identification based structure-thermal analysis of rubber bushing so that credible predictions of mechanical behaviors and thermal effects of rubber bushing during service can be made. The dynamic mechanical property is characterized as frequency-dependent and the corresponding parameters' identifications are carried out through experiment on DMA. A novel approach to estimating the hysteresis damping is proposed on the basis of interaction between carbon black and molecular chain. The quasi-static harmonic excitation tests are carried out to catch the amplitude-dependent hysteresis damping. FEA simulation is employed to predict the rubber's dynamic response and thermal effect under harmonic excitation with the collected parameters demonstrating mechanical properties.

Index terms— rubber bushing; hysteresis damping; parameter identification, temperature distribution.

1 I. Introduction

Quality requirements of rubber bushing, such as stability, vibration transmission, and reliability life are becoming more and more demanding in recently decades for design of vehicle suspension systems (1)(2)(3). Rubber elements are the cheapest and most recommended parts when a vibration isolator with certain stiffness is required (4,5). Furthermore, rubber bushing are highly acceptable for reducing noise transmission, accepting misalignment of axes and accommodating oscillatory motions, etc (6). Rubber bushing can be found in vehicles, airplanes, and tractors, such as chassis, suspension, engine mount, exhaust muffler support, vibration isolator, etc. A modern transportation vehicle may have more than 30 pieces of elastomeric bushings integrated in its structure.

Due to the nonlinear force-deflection relationship, the credible prediction of the mechanical behavior and math model of the rubber is a great challenge. The rubber bushing models of the suspension and the whole vehicle system are generally simple, which are often presented using a linear spring and a viscous dashpot connection in parallel or in series. Nevertheless, in comparison with other materials, the mechanical properties of rubber are very complicated. The forces-displacement and momentrotation relationships are characterized as nonlinear and time dependent (7), thus, the non-linear hysteresis behaviors of rubber bushing and the frequencydependent loss modulus should be included. Due to its nonlinearities, the cumulative hysteretic energy accumulation inside the elastomeric bushing can cause its mechanical properties to change significantly at various temperatures (8). The changes of carbon black concentration, filler's structure, processing and curing affect the dynamic properties, such as modulus and damping response of rubber (9), this makes the test procedure and instruments used for measuring important in determining the corresponding material parameters (10). Especially, the characteristics of time-dependent force-deflection relationship of rubber bushing should take into account preload, excitation

2 II. PRINCIPLE OF MODEL CONSTRUCTION AND CONSTITUTIVE RELATIONSHIP

43 amplitude and excitation frequency in order to present the superposition of elastic force, viscoelastic force and
44 friction force (11).

45 In most of the published researches about rubber's behaviors or models of suspension components, the thermo-
46 dynamical effects upon dynamic excitation received few attention, especially the thermal contribution from the
47 hysteresis damping (12). The primary energy loss in rubber bushing upon harmonic excitation is attributed to the
48 viscoelastic-frequency dependent behaviors commonly represented by spring and dashpot elements in classical
49 models. The second energy loss resulted from the hysteresis damping which is attributed to the nearly rate-
50 independent internal material friction between molecular chains and carbon black particles (13). The composition
51 of rubber and properties of fillers determined the ratio of two types of damping and its rough quantification is out
52 of the discussion of this paper (1). The effect of hysteresis damping on the energy dissipation can be fully described
53 using the non-ellipse loop obtained from rubber components when viscoelastic behavior is negligible, usually
54 quasi-static harmonic excitation. Plenty of comprehensive researches have been done to identify the behavior
55 of friction-resulted hysteresis damping in the rubber components. Hysteresis damping is slightly mentioned in
56 early classic models characterizing the damping effect of viscoelastic materials since just the frequencydependent
57 dynamic excitation has been investigated.

58 Another widely accepted damping in structural analysis is Rayleigh damping coefficient, which expresses
59 the damping as proportional to mass and stiffness of component, that expression has experimentally validated
60 especially under higher frequency condition (5). Different viscoelastic models are mentioned trying to characterize
61 the dynamic behavior of rubber components and balance the burden of experiment measurement as well as
62 computational complexities. In sum, a good model should be concise enough to match the complicated mechanical
63 properties without bringing in redundant parameters (14).

64 The main purpose of this paper is to predict the structure response and temperature distribution of rubber
65 bushing through combining the heat accumulation caused by viscoelastic and hysteresis damping. Considering
66 the balance of computation complexity of adding more elements, practical applicability and reliability, Berg's
67 model is employed in this paper. The principle of proper selection of elements to represent mechanical and
68 physical properties of rubber without bringing in excessive calculation is discussed. The proposed hysteresis
69 damping upon static loading is modeled with three springs in series connection and then in parallel to another
70 three in series connected springs. Parameter identification is realized by employing the multivariable nonlinear
71 optimization analysis to guarantee the minimum errors of predicted curves against experiment measurements.
72 Quasi-static and dynamic harmonic excitations with ramp frequencies and amplitudes are applied on the rubber
73 components to represent amplitude dependency of stiffness and damping. With the identified parameters, the
74 dynamic behavior of rubber bushing under harmonic excitation is simulated in COMSOL Multi-physics, which
75 tallies with the expected distribution. Furthermore, the estimation of temperature distribution is presented with
76 great satisfaction. Many models are propose dtrying to accurately reproduce viscoelastic materials' mechanical
77 behaviors using lumped or discrete springs and dashpots (15,16).

78 2 II. Principle of Model Construction and Constitutive Rela- 79 tionship

80 In the commercial software like Abaqus, the generalized Maxwell model using in-series connection of spring and
81 dashpot is recommended to properly represent frequency-dependent dynamic behaviors of rubber. Berg's three
82 branches model (Fig. 1) incorporating the comprehensive effect of elasticity, viscosity and especially friction
83 effect is a great progress characterizing the amplitude-related hysteresis damping of rubber component upon
84 static loading conditions. The total force of applied uniaxial load is shared by the three branches while each
85 branch displays the individual strain. Spring elements k_2 is selected to represent the elastic behavior of rubber
86 busing, especially the modulus of viscoelastic material after infinite relaxation time (branch 1). Spring elements
87 k_1 and dashpot in series forms Maxwell model (branch 2) which describes the attributes of the amplitude and
88 frequency dependency of viscous damping. Maxwell module can properly predict frequency-dependent stiffness
89 and damping properties of rubber components but not applicable for higher frequencies excitation and constant
90 stress conditions. The third branch is a friction element which describes static friction (hysteresis damping)
91 F_f caused by the relative movement between carbon black and molecular chain. This construction leads to a
92 nonlinear reproduction of the parameter dependency of hysteresis damping and dynamic stiffness in a large range
93 of frequency.

94 a) Quasi-Static Loading(Hysteresis Damping)

95 In Berg's model, a pure algebraic relationship between displacement and friction force is set after configuring
96 the turning point of hysteresis branches (17). The stiffness increases from the lower turning point to the upper
97 turning point representing the auxiliary stiffness induced by the commonly hysteresis harshness. Although the
98 algebraic approach describes the amplitude dependency of stiffness well, it's short of comprehensive coverage of
99 the stiffness variation at every stage of loading and difficult to formulate the random excitation, the latter case
100 is also commonly used in reality. To avoid this drawback of missing particular stiffness evolution, multiple spring
101 elements with special stiffness value for each stage shown in Fig. 2 are suggested to present the typical static
102 characteristic, hysteresis loop. Similar to the bilinear model describing the mechanical properties of elasticplastic
103 materials, the nonlinear stiffness in the static force deflection stage can be simulated step by step using tri-linear

104 model.) ? (? b) ? (? b) ? (? b) ? (? b 2 ? K 2) ? (? K 2) ? (? K 2) ? (? K 2) ? (? K 2 ? K E 5 4 5 4 3
 105 4 2 3 3 1 2 2 2 5 6 2 5 2 4 5 2 4 2 3 4 2 2 2 3 2 1 2 2 2 1 1 f ? ? ? ? ? + ? + ? ? ? ? ? + ? + = (1)

106 The typical S-shaped force-deflection curve also presents larger elastic elongation accompanying the stiffness
 107 reduction again, which is named as Mullins effect, it explains the micro-level damage mechanisms of rubber
 108 subjected to large strain (18). The rate-independent response upon static excitation is the crucial phenomenon
 109 in modeling internal material friction force and exploring the corresponding hysteresis damping. Under static
 110 or quasi-static conditions, time independent and amplitude dependent hysteresis loops are reported in plenty of
 111 literatures, even a change of magnitude of deformation rate couldn't lead to significant variation of the hysteresis
 112 loops. This interesting conclusion indicated that the widely accepted model of viscoelastic material is insufficient
 113 to characterize the quasi-static force-deflection response of rubber bushing. Therefore, the proposed tri-linear
 114 model of springs seems to coherently represent the response of rubber component due to the fact that the stiffness
 115 relaxation, hardening and relaxation occur with the ramping of strain. Furthermore, the tri-linear model can be
 116 adjusted according to the turning point of stiffness if more complicated hysteresis loop is produced in reality.

117 The mechanism of stiffness hardening and relaxation received great attention and the commonly accepted
 118 statement can be explained from the relative motion between molecular chains and carbon black particles. It is
 119 well known that tiny carbon black particles are frequently added into polymer to enhance materials' damping,
 120 stiffness and abrasion resistance. Agglomerates of carbon black particles are linked together by those molecular
 121 chains of polymer of different lengths. Irreversible slipping process between polymer molecule chains and fillers
 122 can happen when the critical deformation of chain is reached. From the force-deflection test, the reduction
 123 of stiffness happened over a large range of strain, which depends on characters of different chain lengths. For
 124 molecular chain with different lengths, slipping process starts at different critical stretch. Furthermore, with the
 125 additional increase of strain, the relative slipping among carbon black agglomerates is stimulated when the elastic
 126 limit of those filler particles is exceeded (14,19). Another logical explanation focuses on recoverable straightening
 127 and rupture of molecule chains subjected to recycle loading. Molecular chains cluster are partially trenced
 128 straight while remaining molecular chains are still in relaxation because of the different lengths and different
 129 elastic limits of the molecular chains. It is assumed that the movement of carbon black particle is instantaneous
 130 and molecular chains are more delayed. During initial loading or under small strain, molecular chains cluster are
 131 mainly slack without any contribution of rubber hardness. When carbon black particle starts move, the stiffness
 132 of rubber increases obviously since more and more molecular chains stretched and starting to undertake load.
 133 Further increase of loading or lager strain push the carbon black particle move more, as a response, molecular
 134 chains cluster will start to break In Berg's model, maximum force and turning point of amplitude is needed to
 135 derive the half of the maximum force which is useful parameter to describe the frequency-independent hysteresis
 136 stiffness. Similarly, Fig 2 also displays four turning points which split the loading and unloading curves into three
 137 pieces. The auxiliary stiffness of hysteresis damping upon static friction effect are represented with spring K 2
 138 and K 5 which are located between turning points and much more hardened than the remaining springs. Due to
 139 the different stiffness of each piece of curve, a tri-linear model with multiply springs K i is suggested, where i=1,
 140 2, 3, 4, 5, and 6. Stresses of different pieces of hysteresis loop should be written as: $3 \ 3 \ b \ K \ + \ = \ ? \ ?$

141 . In order to balance the model complexity and computation efficiency, the six springs stiffness can be simplified
 142 by setting $K \ 2 \ =K \ 5$; $K \ 1 \ =K \ 4$ and $K \ 3 \ =K \ 6$ according to the acknowledged profile of hysteresis curve. The
 143 total energy lost (E f) per cycle caused by hysteretic damping can be produced by calculation of the loop area,
 144 once the elastic limit is reached. Due to different length of molecular chains, the hardening and reduction of
 145 stiffness happens gradually over a certain range of strain, which brings certain difficulty to detect the strain of
 146 turning points. The straightening and breakage of molecular chains are partially reversible during unloading. As
 147 a result, the non-overlapping forcedeflection curves upon loading and unloading caused noticeable static hysteresis
 148 damping. $? \ ? \ ? \ = \ = \ (2)$

149 Where $? , ?$ are total stress, $? \ 1 , ? \ 1$ are stress and strain of Maxwell elements in series with mass, and $? \ 2 , ?$
 150 2 are stress and strain of spring mass elements. The constitutive equation of the standard liner solid is expressed
 151 as Equation (3), $d \ ? \ ? \ ? \ ? \ ? \ k \ (\ k \ dt \ d \ ? \ 2 \ 2 \ 1 \ + \ = \ + \ + \ (3)$

152 The road spectrum of vehicle vibration are collected in time domain and usually transferred to frequency
 153 domain before application and analysis. To facilitate the further application of current model, the harmonic
 154 excitations are assumed in the following discussion, which leads to, $?? \ ik \ ? \ ? \ 1 \ ? \ ? \ k \ k \ ' \ ik \ ' \ k \ ' \ k \ + \ + \ + \ = \ +$
 155 $= \ (5)$

156 Where the The experimental results of rubber components under static load and harmonic excitation are
 157 obtained to identify parameters of each element in the advanced rubber model. All the data measurement are
 158 finished using equipment dynamic mechanical analysis (DMA) which measures the influence of frequencies, time
 159 and temperature on materials mechanical properties. Harmonic excitation operated using this instrument can a)
 160 Friction Force (Hysteresis Damping)

161 In the case of static loads, loading with lower velocity and excitation frequencies are utilized to simulate the
 162 quasi-static loading condition due to impractical static loading. Considering the accuracy and reliability, the
 163 excitation frequencies of quasi-static condition is chosen from $F=0.01$ to $F=0.1$ HZ. The very low frequencies are
 164 required to keep the contribution of viscous damping in a negligible position. The stress is ramped from 0.001MPa
 165 to 0.05MPa to study the amplitude dependency when frequencies are fixed. The corresponding reports about
 166 stiffness, damping, tan delta and amplitude will output automatically as long as the pre-set working condition

3 B) HARMONIC EXCITATION (VISCOUS DAMPING)

167 is reached and being stable. Fig. 4 shows the variation of amplitude of the rubber component is subjected to
168 quasi-static low frequency excitation.

169 The observed stiffness dependency upon excitation amplitudes in Fig. ?? is the well known Payne effect
170 commonly appearing in fillers strengthened rubber compounds. The reduction of stiffness of rubber components
171 with the increasing excitation amplitudes is attributed to the weak van der Waals bonds existing in the
172 agglomerates formed from carbon black particle (20). The recoverable rupture of physical bonds accumulates
173 when imposing higher amplitudes is imposed, resulting in a significant relaxation of stiffness in the macro-level.
174 For the very small amplitude, friction plays dominant contribution to the raise of stiffness. As the amplitude
175 tends to become larger, part of molecular chains break in the micro-level which leads to friction release in macro-
176 level. Considering the quasi-static hysteresis loop and the amplitude dependency of static stiffness, the tri-linear
177 model has been suggested and its coefficients of springs can be estimated using multivariable constrained method.
178 The equation formulated for parameterizing the hysteresis loop is based on the ratio of energy dissipation over
179 total storage energy, Where S' is the area in side of hysteresis loop, and S is the storage energy during loading.
180 As to the reported tan delta of every loading condition, corresponding strain can be collected and the area S'
181 and S can be easily estimated using the Equation (1). There are three parameters to identify, which means at
182 least two groups of data under the same or close excitation frequencies required to implement the optimization.
183 Stiffness before and after the hysteresis harness during quasi-static measurement are set as the initial value for K_1
184 and K_2 . The optimization results are illustrated in Fig. ??b. Note that K_1 , K_2 and K_3 slightly decrease
185 with increasing amplitudes and K_3 is much lower than K_1 , which also agrees well with the previous description
186 of molecular chains. For further calculation, the K_1 , K_2 and K_3 are taken as 3.07MPa, 6.62MPa and 0.02
187 MPa separately. The tan δ is taken as 0.05. It is also reasonable to observe that the fracture of molecular chains
188 causes even more reduction of stiffness than the chains' relaxation.

189 3 b) Harmonic Excitation (Viscous Damping)

190 For the dynamic stiffness besides of the hysteresis damping, the module is a combination of advanced Maxwell
191 system and spring, which means three parameters k_1 , k_2 and c_1 are required to determine the frequency
192 response of dynamic behaviors, see Equation (13). The dimension of the rubber sample used for the DMA test
193 is less than 5mm in thickness and about 10mm in diameter, furthermore, stress higher than 0.1MPa could lead
194 to shift of sample and fail to produce valid data. Thus, the corresponding output amplitude is pretty low in
195 consideration of the sample size and loading restriction. In the modeling of railway and vehicle track interaction,
196 vehicle suspensions are designed to make sure of the effective isolation of vibration when the frequency is below
197 10HZ. Track dynamics gradually play the dominated role than vehicle dynamics when the frequencies reached
198 20HZ. Under this condition, low frequencies force-deflection relations should be discussed here for stability and
199 passenger comfort(3). In the current parameterization, frequencies of harmonic excitation are ramped from
200 1HZ to 100HZ to balance the time consuming data collection and representativeness over the large range of
201 frequencies. In order to investigate the amplitude dependency of viscous damping, the stresses of each frequency
202 is run from 0.01MPa to 0.1MPa. For low frequencies such as 0.001HZ and high frequency such as 100HZ, the
203 measurements are impeditive and some data are missing due to the testing condition of stresses and frequencies
204 are not applicable to this sample. The overall variation of dynamic stiffness and damping over amplitudes and
205 frequencies are plotted in Fig. 4. With the increase of frequencies, amplitude of the same stress will decrease while
206 dynamic stiffness keeps decreasing. As a comparison, the damping presented a peak when the excitation frequency
207 $F=30$ HZ in spite of the variation of amplitude. For more in-depth discussion, outputs are sketched for more direct
208 demonstration. It can be concluded from Fig. 5 that both the storage modulus and dynamic stiffness increase
209 almost linearly with frequency and strain, which clearly illustrated the amplitude and frequencies dependency of
210 dynamic behaviors. The almost linear increase of storage modulus also is proportional in line with energy input
211 As discussed in Fig. 4, the energy dissipation presented with tan delta does not monotonously varying with the
212 frequencies or amplitude. Similarly, note that the incongruous increase of loss modulus, damping and tan delta at
213 frequencies $F=30$ HZ in Fig. ??, that abrupt increase becomes even more obvious at a slightly higher amplitude.
214 In sum, loss modulus increases with amplitude and damping variation displays the same tendency. In the range
215 of lower frequencies, the increase with strain is slight and the increase of frequencies only slightly affects the
216 position of those lines in Fig. ?. It is noticeable that the tan delta data at lower excitation frequencies can be
217 almost fitted using straight horizontal lines. Similar phenomenon is also observed in the quasi-static deformation
218 when harmonic excitation is as low as 0.01HZ. The linear fitting curve for tan delta upon quasi-static loading
219 gives slope- 2.12363×10^{-4} , which illustrated that ratio of hysteresis damping to the energy input is independent
220 of the excitation frequencies at quasi-static or lower frequency condition. It must be mentioned that quasi-static
221 stiffness and tan delta should be excluded to identify the parameters in Equation (???) describing the dynamic
222 behaviors. As to damping, it increases with frequencies gradually at the very beginning and abruptly reaches
223 maximum at frequency around 30HZ. After this peak, damping decreases with continually rising frequencies.
224 This dependency become seven more obvious with the increase of amplitude. The dependency of damping on
225 frequencies can be split into three stages according to the mechanism in the macro-level. All molecular chains of
226 rubber response to harmonic excitation of pretty low frequency changes almost simultaneously with the load and
227 barely lag of phase. This stage is commonly named as high elastic rubber and display limited energy dissipation,
228 which manifests as lower damping and tan delta. While, molecular chains can totally lag behind the deformation

of rubber components when harmonic excitation frequencies are within a high range, such as more than 50HZ in the current case. Also, the rubber components upon high frequencies excitation are close to glass state and display much less energy dissipation. A more complicated dynamic behavior is the response of rubber upon the medium range frequencies excitation, for example 30HZ in Fig. ???. In that case, part of molecular chains can follow the macro-deflection of rubber, at the same time, resulting in a larger lag of angle delta and higher energy dissipation.

In order to reproduce the variation of stiffness and damping response with the frequencies, there are three parameters k_1 , k_2 and c_1 needed to be identified with the experimental measurement subjected to medium and high-frequency harmonic excitation. From previous analysis, an optimization function should be formulated to satisfy the frequency-dependent stiffness and tan delta together. The multivariable equation is presented in Equation (??), $\tan \delta = \frac{c_1 \omega}{k_1 + k_2 \omega^2} + \frac{k_1 \omega^2}{k_1 + k_2 \omega^2} \tan \delta_0$ (7)

Dynamic stiffness is defined as $\frac{F}{\Delta} \text{ [dyn]}$ $\tan \delta = \frac{c_1 \omega}{k_1 + k_2 \omega^2} + \frac{k_1 \omega^2}{k_1 + k_2 \omega^2} \tan \delta_0$. Tan delta is less than 0.2 in almost all testing conditions, therefore, $\text{dyn } k$ is approximate to k' with error less than 2%. Furthermore, k' is close to $2k$ as long as the excitation frequencies are pretty low, finally, dynamic stiffness $\text{dyn } k$ is selected to place the initial value of $2k$. Considering the friction effect of rubber upon the quasi-static deformation and its contribution to the hysteresis stiffness, the data used for the dynamic behavior's parameter identification should reduce the quasi-static stiffness and tan delta. The decrease of hysteresis stiffness becomes weak if the amplitude of dynamic excitation is set as pretty large since the reduction from the rupture of physical of bond between carbon black particles is only confined within a certain range of strain. The static stiffness variation upon amplitude is usually described exponentially or hyperbolically decreasing model. It can be concluded that the static stiffness with the auxiliary of friction effect can be treated as constant as the amplitude at higher frequencies is in hundreds. The initial value of k_1 usually starts from 0.7 dyn k to accelerate the optimization calculation. Damping coefficient is relative low and 1000N/m should be a good initial point. 7 shows the comparison of experiment curve against predicted curve plotted with the parameters obtained from optimization. The stress for this group of data is set as 0.05MPa. It is commonly to have the much better fitting for dynamic modulus than the tan delta fitting. Approximate correction can minimize the relative error of tan delta fitting, while that barely changes the parameter identification results. The fitting results in Fig. 7 give $k_1 = 0.49\text{MPa}$; $k_2 = 1.009\text{MPa}$ and $c=0.028\text{MPa.t}$. The obtained stiffness k_2 is pretty close to the dynamic stiffness when excitation frequency $f=1\text{HZ}$, that result is verified against the proper assumption of initial values for optimization procedure. It can be seen easily that dynamic modulus increases with frequencies and there is a peak of damping with the increasing of frequency. As discussed from previous amplitude dependency, the dynamic stiffness and damping is generally amplitude dependent. Actually, DMA tests over a stress range 0.01MPa to 0.1MPa are carried out to found the best data for parameter identification, which is realized with the error analysis. To verify the optimal stress and frequency excitation condition to collect data for accurate model parameter identification, the three-dimensional diagram of dynamic stiffness and tan delta error varying with increasing amplitude and frequency are plotted in Fig. 8. As to the medium frequencies excitation, dynamic modulus and tan delta almost reach the maximum value, then, relative error of dynamics stiffness is minimized due to the absolute increment of stiffness. A better selection of excitation amplitude is located in the central part of the amplitude spectrum. The error analysis results indicated that optimization with experiment data upon lower stresses is poorer compared with that from medium or higher stress excitation. This may be attributed to the error of hysteresis stiffness estimated for quasi-static condition, which highly affects dynamic output upon lower frequencies excitation. While the tan delta of quasi-static loading is barely varied with amplitudes, thus, the Tan delta representing dynamic loss shows no obvious variation of relative error changing with amplitudes. As illustrated, the determinacy of frequency becomes more obvious in determining the error, which suggests the medium frequency as better experiment data range. Since the error distribution characteristics of dynamic stiffness and tan delta are consistent in the optimal selection of excitation stresses and frequencies for parameter identification, harmonic excitation are carried out with stresses set as 0.05MPa. Higher stress and higher frequency excitation condition is kind of out of the service scope of DMA test equipment, Again, excitation of too lower or too higher frequency leads to higher relative error, that makes the medium frequencies as much more cautious selection to collect the reliable experiment data.

4 IV. The fea Analysis about

Temperature Distribution

The FEA simulation with multi-physical COMSOL will be used as an instructive prediction about the heat generation magnitude and temperature distribution. The simulation includes two steps, the first is the force-frequency analysis to estimate the heat generation rate and the next step is the temperature distribution at steady state. The mechanical properties of viscoelastic materials are expressed in Prony series since the commonly recommended generalized Maxwell model introducing many parameters. The general Prony series expression representing shear stress relaxation modulus is Figure ?? : The effect of total strain and strain rate R (mm/s) on the stiffness of rubber It is important to claim that the heat generation rate comes from two aspects, one is the viscoelastic damping, and the other one is the hysteresis damping. From the specification of viscoelastic material, the heat generation results of force-frequency analysis merely presenting the viscoelastic damping. Thus, the hysteresis damping describing the friction effect can be set as heat source and the amplitude is determined

5 V. CONCLUSION

291 from structure analysis. To get more precise prediction about temperature distribution, Hot Disk thermal analysis
292 instrument based on the transient plane source (TPS) method is applied to measure the thermal diffusivity and
293 thermal conductivity (Table 1).The probe of the instrument can provide heat source and record the temperature
294 variation with time. The density and heat capacity are estimated using the mixing rule with the weight percentage
295 of polymer and carbon black, which is estimated with thermal gravity analysis (TGA). The loading frequency is
296 set as 9.0134 HZ according to the time history of the loading from the field test. Fig. 10 shows the structure and
297 thermal coupling analysis results produced by COMSOL software. The energy loss coming from the viscoelastic
298 damping is presented as the power dissipation density (W/m^3) which plays as the major heat source for
299 temperature rising. The secondary heat source is hysteresis damping which is defined as constant heat flow since
300 the displacement amplitude is determined under specified load. The results display that the two faces of the
301 rubber bushing accumulated maximum power dissipation density, in turn, the temperature of that two areas
302 are higher. Rent (21) found the center of the bonded surface displays maximum compressive stress which is
303 almost twice the average and again even much higher than the edges. The current FEA results display the same
304 tendency of stress and temperature distribution which are decreasing from the central zone to the edge of the
305 rubber block.

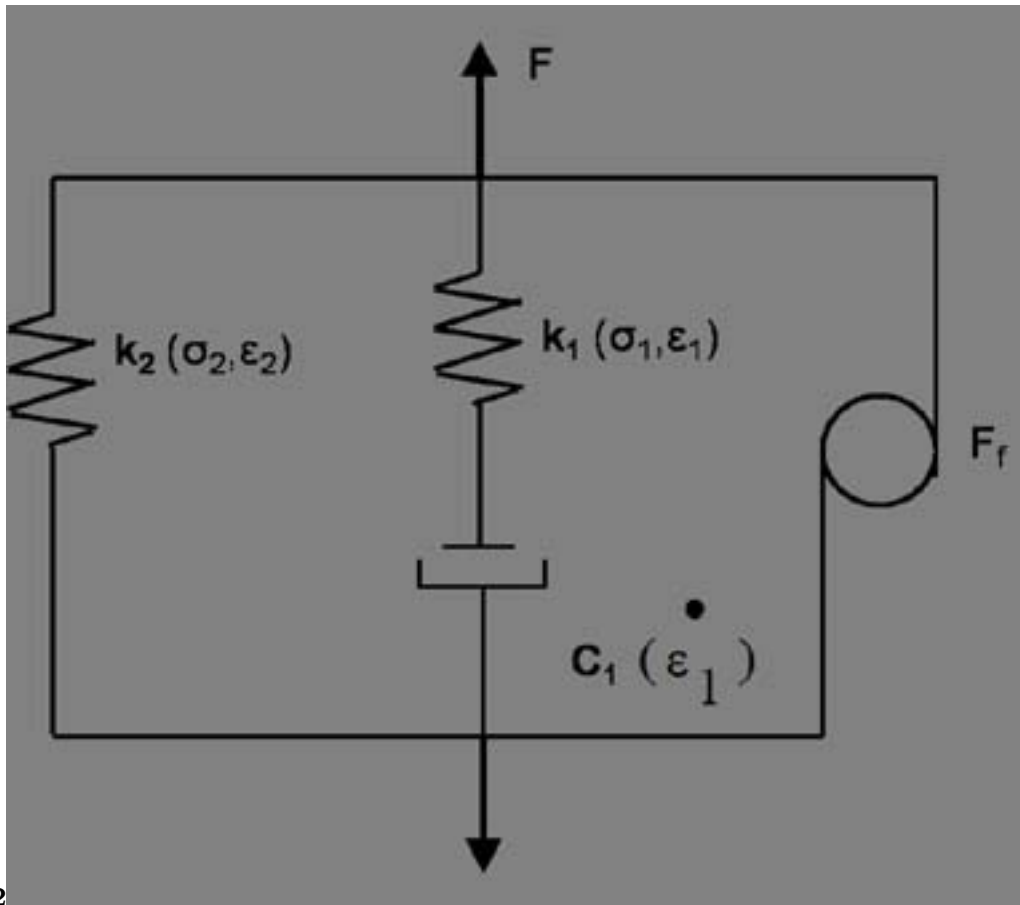
306 5 V. Conclusion

307 A standard linear model parallel to a friction element is employed in this paper to represent the dynamic and
308 quasi-static mechanical properties of rubber with high accuracy and credibility. Spring elements with different
309 stiffness at corresponding stages of deformation are presented to frame the hysteresis damping subjected to the
310 static loading. The tri-linear model is more specific in emphasizing the stiffness hardness and relaxation for
311 each piece of the loop. DMA of different frequency and stress are measured and the model is parameterized
312 using multivariable constrained optimization where data from medium stresses and frequencies are suggested to
313 obtain the optimal dynamic parameters to controls the error. Observed from experimental measurements, the
314 amplitude dependency of hysteresis stiffness illustrates exponential decrease while the dynamic stiffness of rubber
315 increases with the amplitude. Parameter identification procedures are computationally inexpensive and easily
316 applicable, along with the error erroneous analysis. The most adaptable experimental conditions are suggested
317 to demonstrate the model that most precisely matches the real rubber mechanical performance. The powder
318 dissipation density is obtained and its effect on temperature distribution has been analyzed. In the future, the
thermal effect on life expectation of rubber bushing will be investigated. ^{1 2 3 4}



1

Figure 1: Figure 1 :



2

Figure 2: Figure 2 :

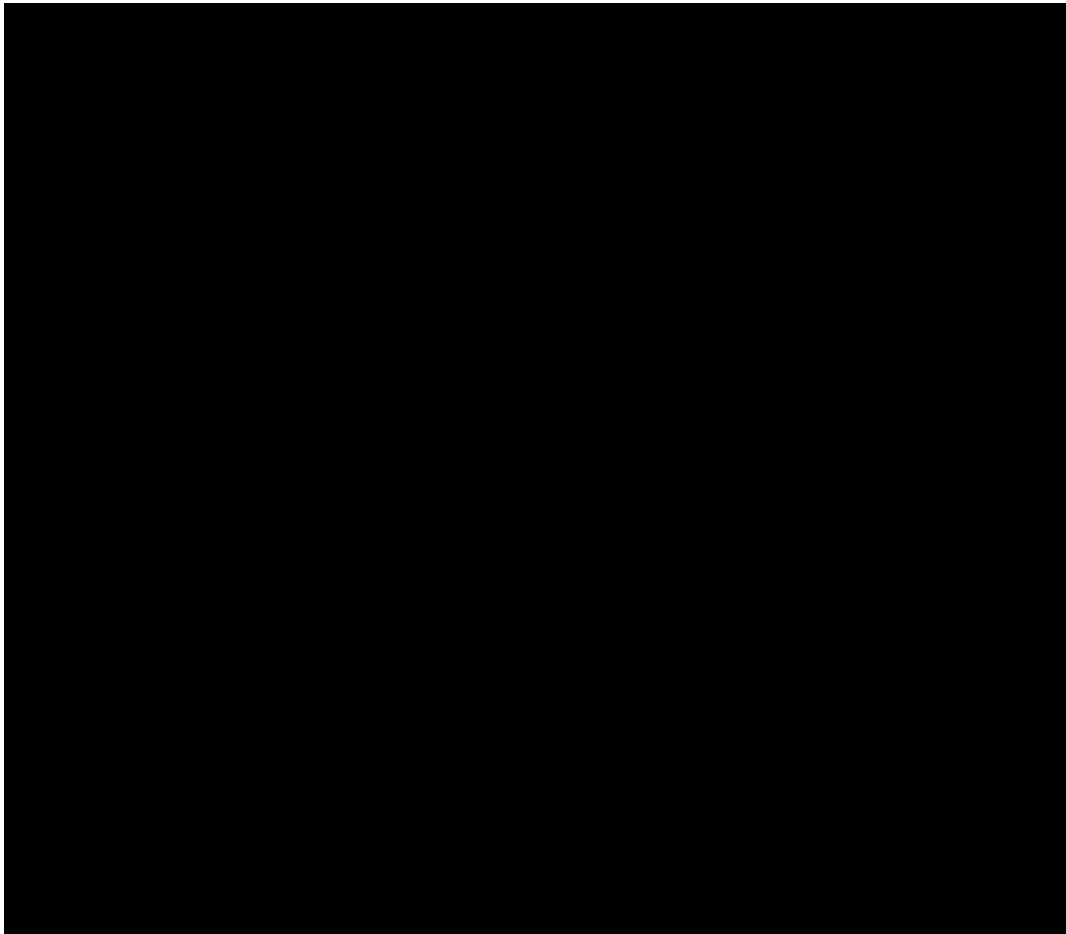


Figure 3:

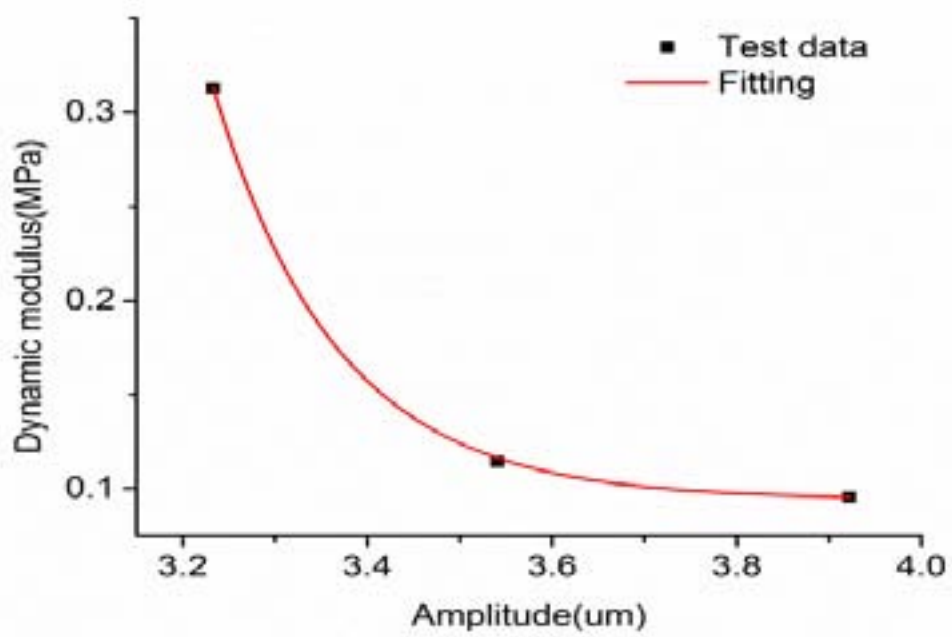


Figure 4:

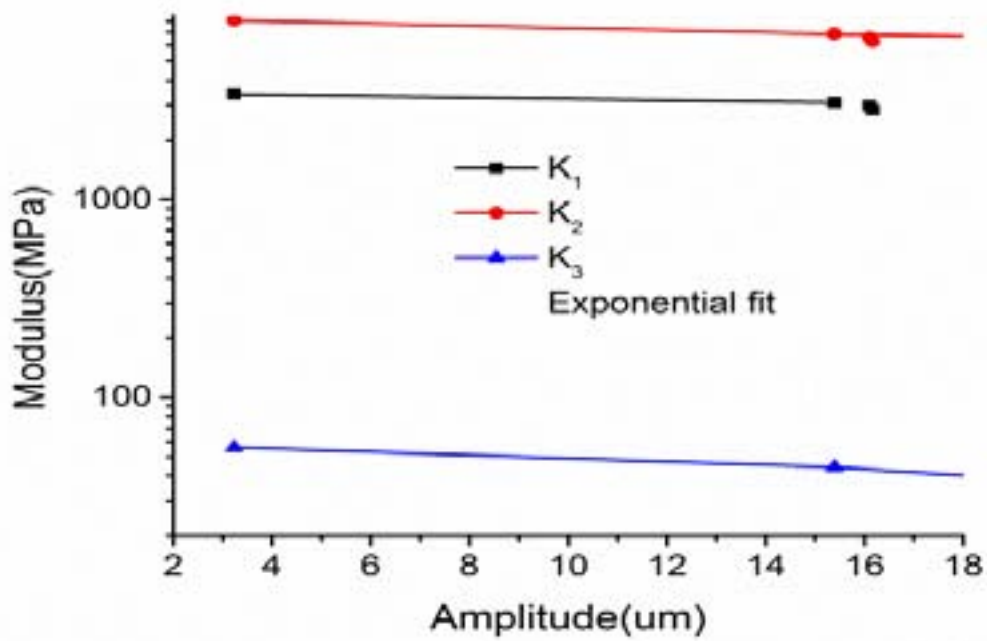


Figure 5:

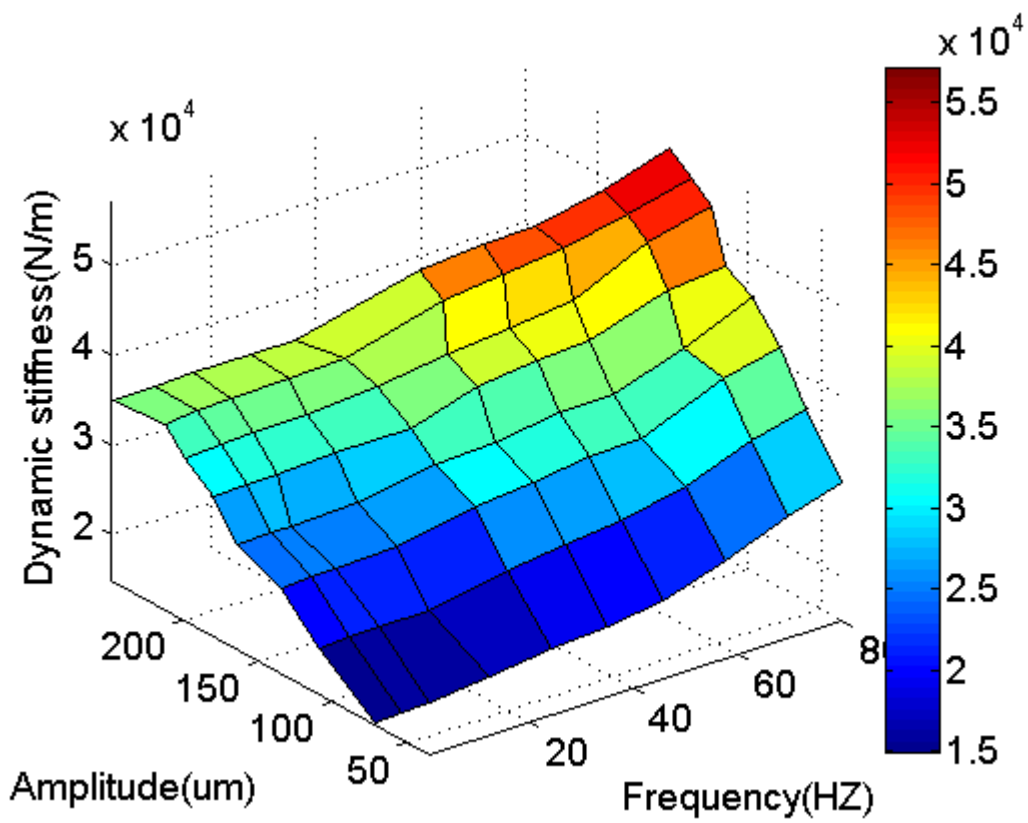
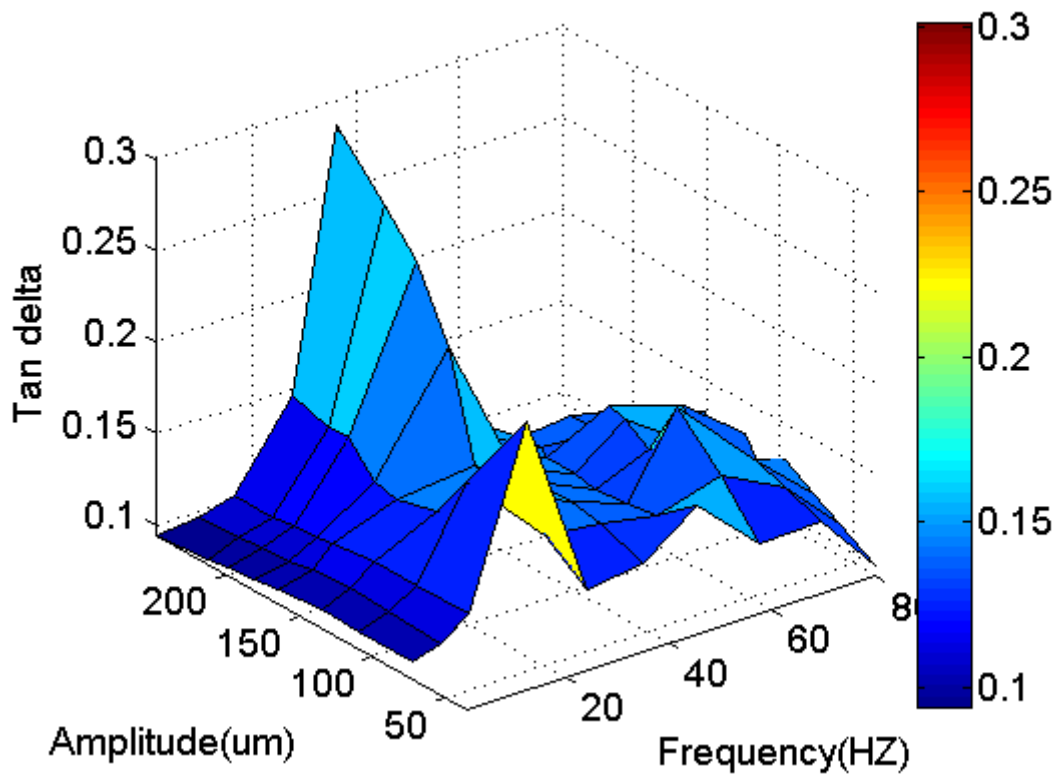
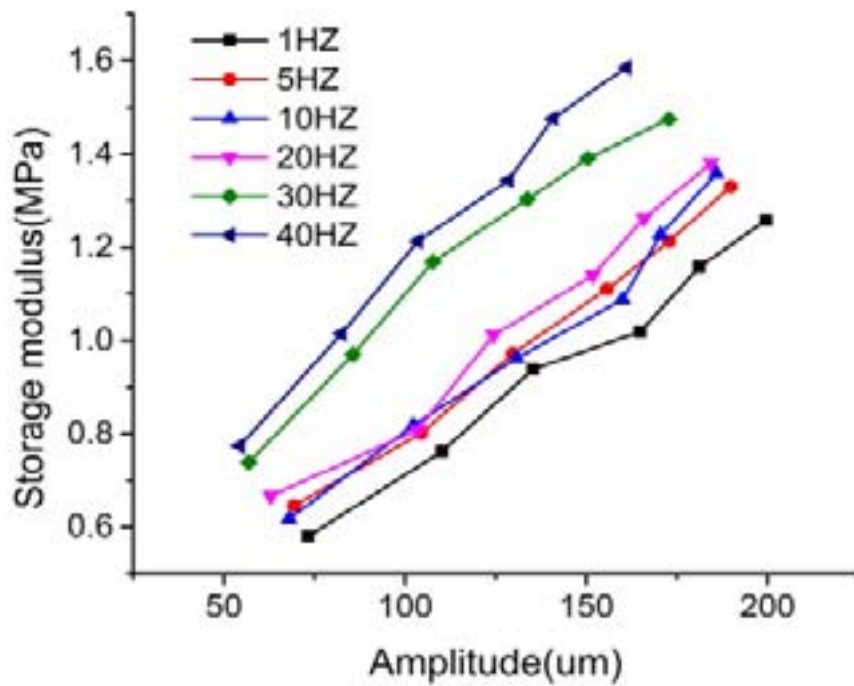


Figure 6:



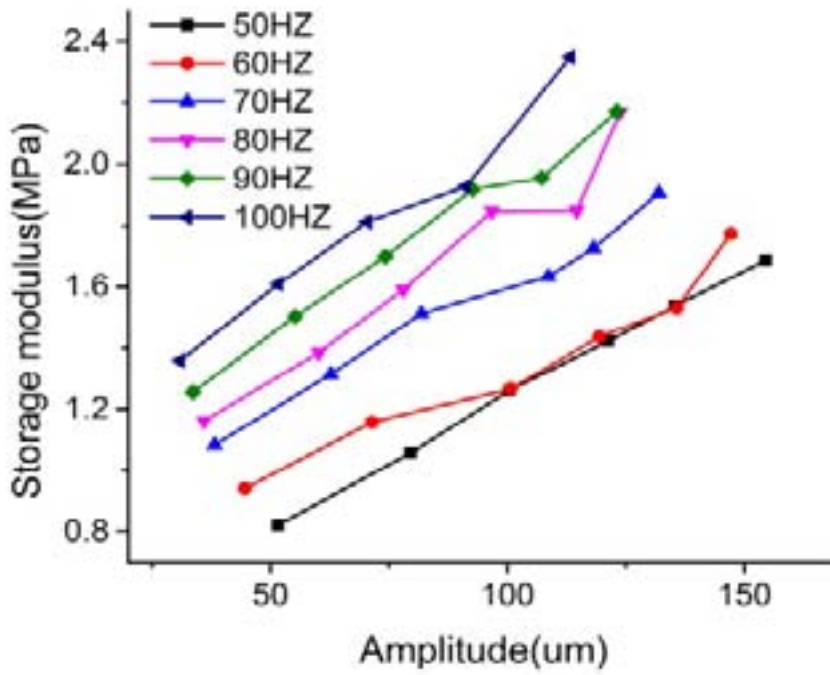
1

Figure 7: $r = 1$ C



34

Figure 8: Figure 3 : 4 Viscoelastic



4

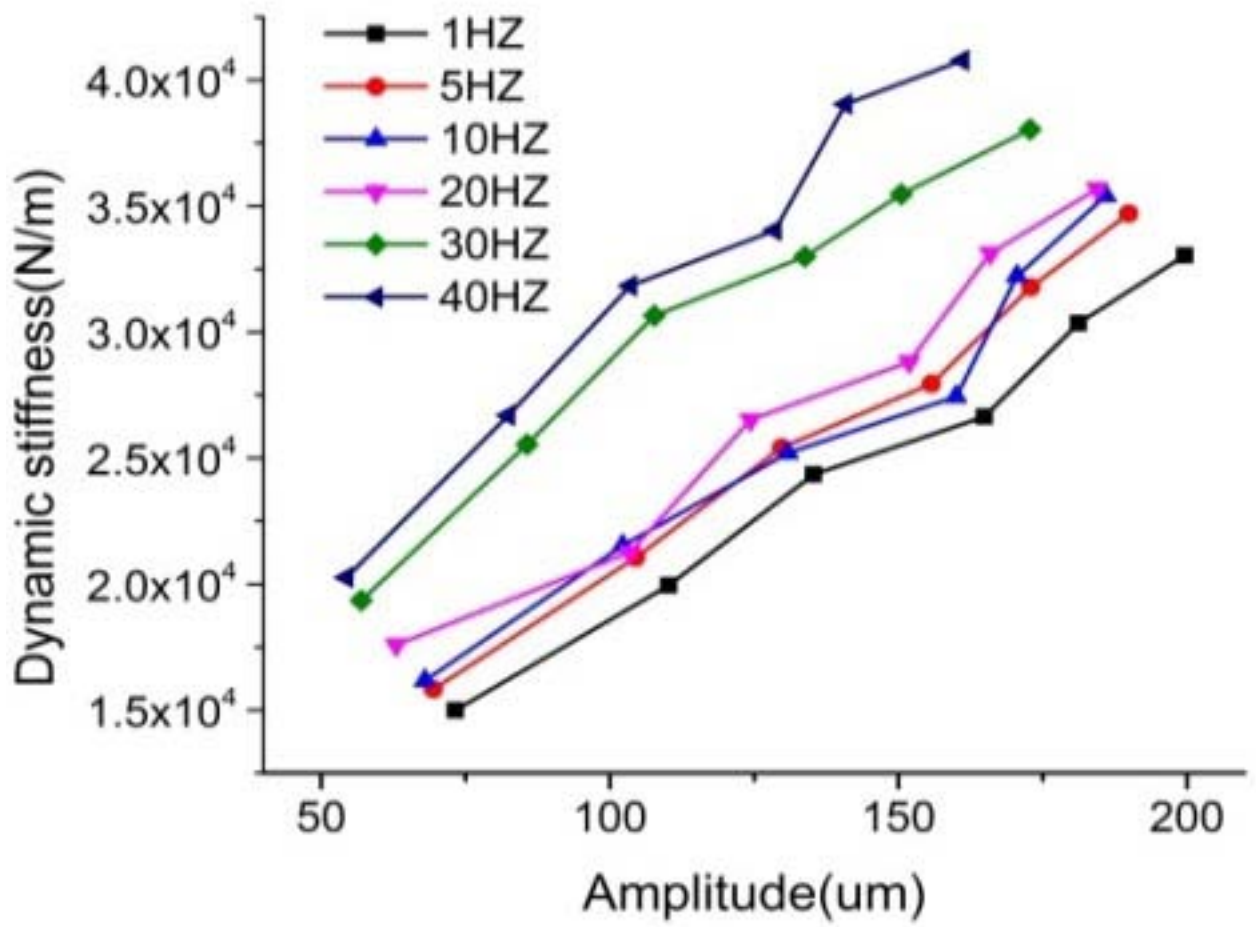
Figure 9: Figure 4 :

¹© 2014 Global Journals Inc. (US)

²Viscoelastic Parameter Identification based Structure-Thermal Analysis of Rubber Bushing

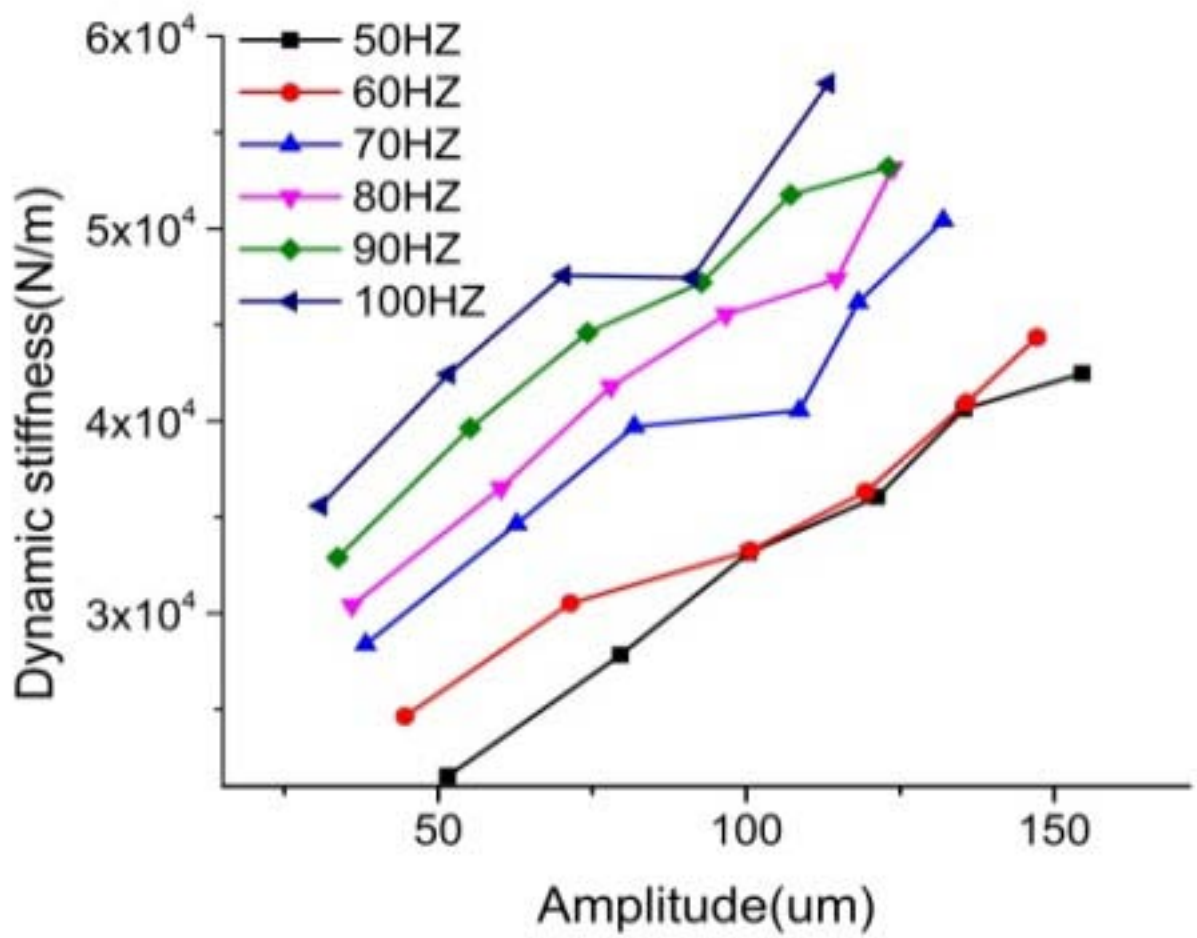
³Year 2014 Viscoelastic Parameter Identification based Structure-Thermal Analysis of Rubber Bushing

⁴Year 2014 Viscoelastic Parameter Identification based Structure-Thermal Analysis of Rubber Bushing



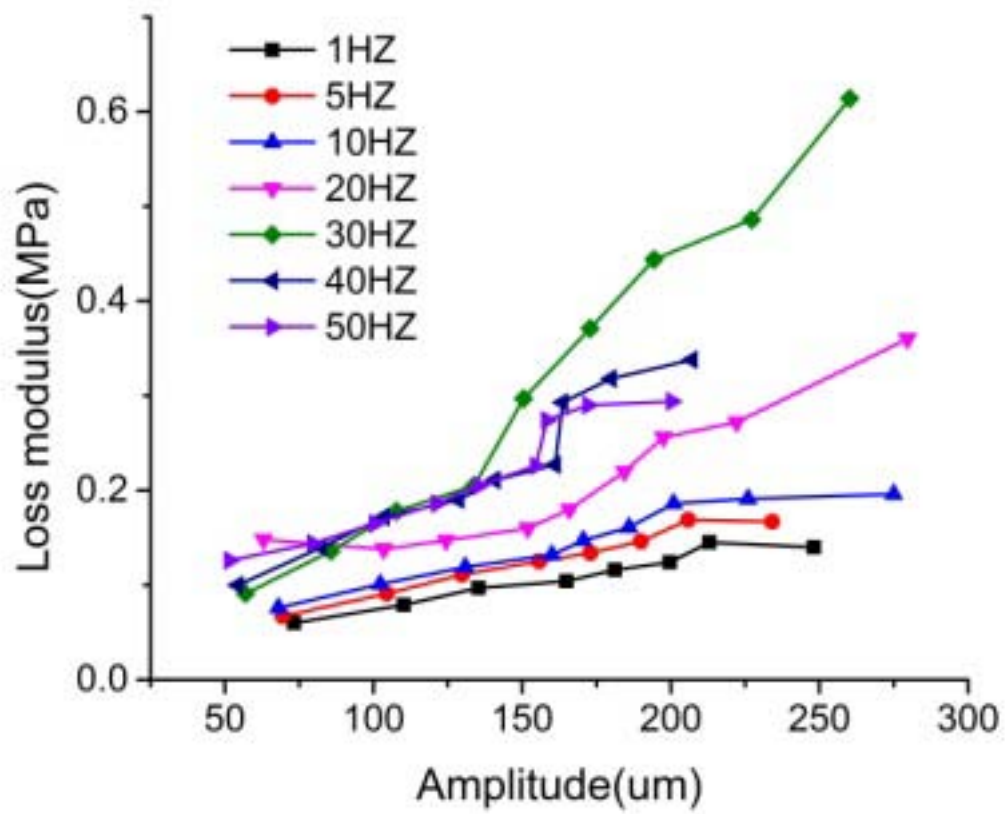
5

Figure 10: Figure 5 :



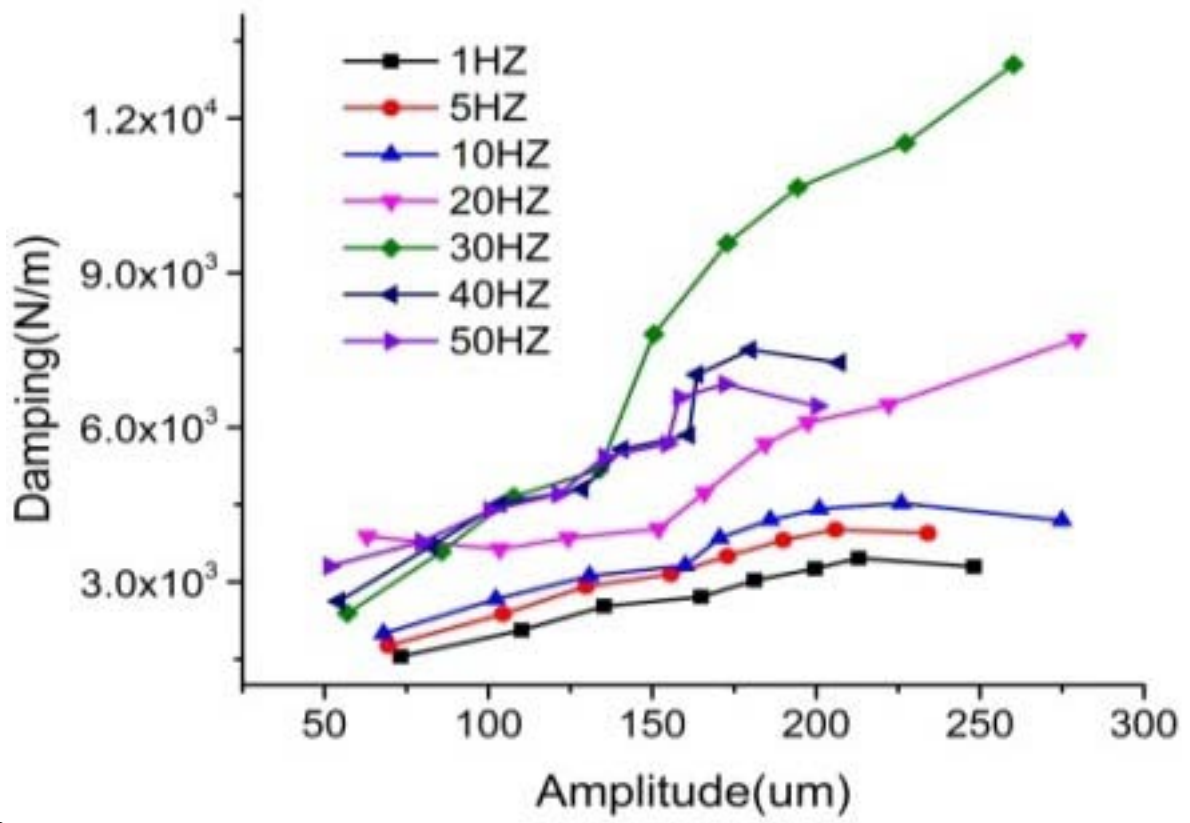
66

Figure 11: Figure 6 : 6 Viscoelastic



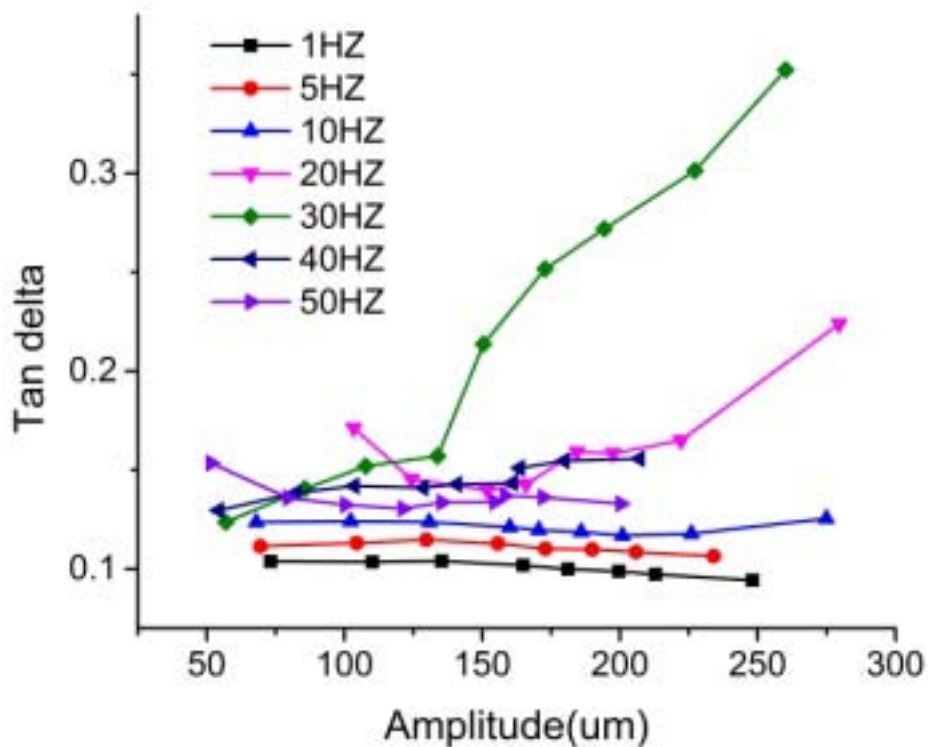
7

Figure 12: Figure 7 :



8

Figure 13: Figure 8 :



10

Figure 14: Figure 10 :

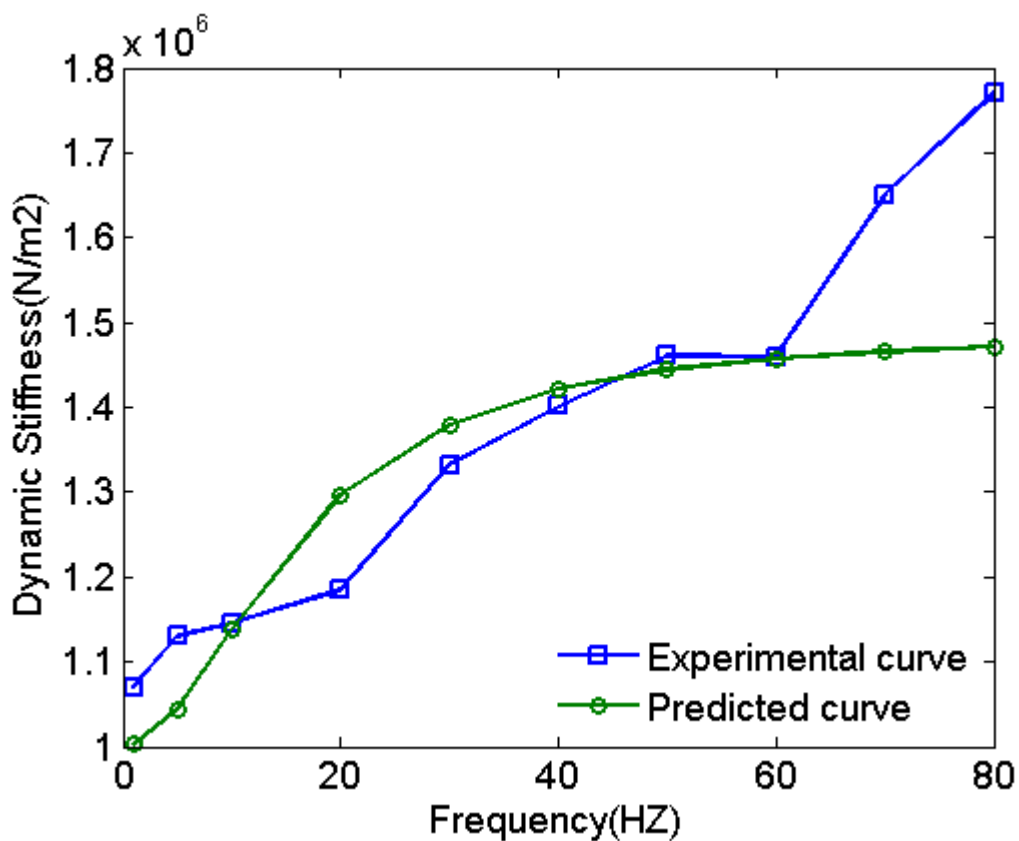


Figure 15:

1

Density	Heat Capacity	Thermal diffusivity	Thermal conductivity	Heat transfer coefficient
952.54 (Kg/m ³)	1611.44 (J/Kg.K)	0.202 (mm ² /s)	0.343 (W/m.K)	10 (W=(m ² /K))

Figure 16: Table 1 :

319 Where G_i is the relaxation time for per series components, τ (G is the long term shear modulus when t
320 is approximated to infinite and
321 τ . In the current standard linear model, $N=1$, and

322 [Berg ()] ‘A model for rubber springs in the dynamic analysis of rail vehicles’. M Berg . *Proceedings of the*
323 *Institution of Mechanical Engineers* 1997. 211 (2) p. . (Part F: Journal of Rail and Rapid Transit)

324 [Sayyaadi and Shokouhi ()] ‘A new model in railvehicles dynamics considering nonlinear suspension components
325 behavior’. H Sayyaadi , N Shokouhi . *International Journal of Mechanical Sciences* 2009. 51 (3) p. .

326 [Berg ()] *A non-linear rubber spring model for rail vehicle dynamics analysis. Vehicle system dynamics*, M Berg
327 . 1998. 30 p. .

328 [Gil-Negrete et al. ()] ‘A simplified methodology to predict the dynamic stiffness of carbon-black filled rubber
329 isolators using a finite element code’. N Gil-Negrete , J Vinolas , L Kari . *Journal of Sound and Vibration*
330 2006. 296 (4) p. .

331 [Kaliske and Rothert ()] ‘Constitutive approach to rateindependent properties of filled elastomers’. M Kaliske ,
332 H Rothert . *International Journal of Solids and Structures* 1998. 35 (17) p. .

333 [Bergström and Boyce ()] ‘Constitutive modeling of the large strain time-dependent behavior of elastomers’. J
334 Bergström , M Boyce . *Journal of the Mechanics and Physics of Solids* 1998. 46 (5) p. .

335 [Dean et al. ()] ‘Determination of non-linear dynamic properties of carbon-filled rubbers’. G Dean , J Duncan ,
336 A Johnson . *Polymer testing* 1984. 4 (2) p. .

337 [Alonso et al. ()] ‘Development of a rubber component model suitable for being implemented in railway dynamic
338 simulation programs’. A Alonso , N Gil-Negrete , J Nieto , J Giménez . *Journal of Sound and Vibration* 2013.

339 [Roland ()] ‘Dynamic mechanical behavior of filled rubber at small strains’. C Roland . *Journal of rheology* 1990.
340 34 p. 25.

341 [Luo et al. ()] ‘Dynamic simulation studies and experiments on rubber structures used in rail vehicles’. R K Luo
342 , X Wu , W J Mortel . *Proceedings of the Institution of Mechanical Engineers* 2013. 227 (1) p. . (Part F:
343 Journal of Rail and Rapid Transit)

344 [Medalia ()] *Effect of carbon black on dynamic properties of rubber vulcanizates. Rubber Chemistry and*
345 *Technology*, A Medalia . 1978. 51 p. .

346 [Kadlowec et al. ()] *Elastomer bushing response: experiments and finite element modeling. Acta mechanica*, J
347 Kadlowec , A Wineman , G Hulbert . 2003. 163 p. .

348 [Gent et al. ()] ‘Interfacial stresses for bonded rubber blocks in compression and shear’. A Gent , R Henry , M
349 Roxbury . *Journal of Applied Mechanics* 1974. 41 (4) p. .

350 [Payne and Whittaker ()] *Low strain dynamic properties of filled rubbers. Rubber chemistry and technology*, A
351 Payne , R Whittaker . 1971. 44 p. .

352 [Stein et al. ()] ‘Modeling and computation of shakedown problems for nonlinear hardening materials’. E Stein ,
353 G Zhang , Y Huang . *Computer methods in applied mechanics and engineering* 1993. 103 (1) p. .

354 [Knothe and Grassie ()] *Modelling of railway track and vehicle/track interaction at high frequencies. Vehicle*
355 *system dynamics*, K Knothe , S Grassie . 1993. 22 p. .

356 [Pan and Chai ()] ‘Modelling of rubber mounts and applications for time response analysis of dynamic systems
357 including elastomerics’. X-Y Pan , G-Z Chai . *International Journal of Vehicle Design* 2009. 49 (4) p. .

358 [Stein et al. ()] ‘Shakedown with nonlinear strain-hardening including structural computation using finite ele-
359 ment method’. E Stein , G Zhang , J A König . *International Journal of Plasticity* 1992. 8 (1) p. .

360 [Mullins ()] *Softening of rubber by deformation. Rubber Chemistry and Technology*, L Mullins . 1969. 42 p. .

361 [Dannenberg ()] *The effects of surface chemical interactions on the properties of filler-reinforced rubbers. Rubber*
362 *Chemistry and Technology*, E Dannenberg . 1975. 48 p. .

363 [Tarrago et al. ()] ‘Viscoelastic models for rubber mounts: influence on the dynamic behaviour of an elastomeric
364 isolated system’. Garcia Tarrago , M Gil-Negrete , N Vinolas , J . *International Journal of Vehicle Design*
365 2009. 49 (4) p. .